Evaporation-Induced Assembly of Quantum Dots into Nanorings

Jixin Chen, Wei-Ssu Liao, Xin Chen, Tinglu Yang, Stacey E. Wark, Dong Hee Son,* James D. Batteas,* and Paul S. Cremer*

Department of Chemistry, Texas A&M University, College Station, Texas 77843

ABSTRACT Herein, we demonstrate the controlled formation of two-dimensional periodic arrays of ring-shaped nanostructures assembled from CdSe semiconductor quantum dots (QDs). The patterns were fabricated by using an evaporative templating method. This involves the introduction of an aqueous solution containing both quantum dots and polystyrene microspheres onto the surface of a planar hydrophilic glass substrate. The quantum dots became confined to the meniscus of the microspheres during evaporation, which drove ring assembly *via* capillary forces at the polystyrene sphere/glass substrate interface. The geometric parameters for nanoring formation could be controlled by tuning the size of the microspheres and the concentration of the QDs employed. This allowed hexagonal arrays of nanorings to be formed with thicknesses ranging from single dot necklaces to thick multilayer structures over surface areas of many square millimeters. Moreover, the diameter of the ring structures could be simultaneously controlled. A simple model was employed to explain the forces involved in the formation of nanoparticle nanorings.

KEYWORDS: ring · CdSe quantum dots (QDs)/nanocrystals · nanoparticle self-assembly · evaporative templating · nanosphere (colloidal) lithography · capillary lithography

Semiconductor and metal nanoparticles can be exploited as building blocks for designing photonic, electronic, and magnetic devices as well as for use in sensing and optical applications.[1−5] Patterned arrays of nanoparticles can even serve as platforms for studying fundamental physical chemistry and molecular interactions.[4,6−8] In particular, the fabrication of ring structures has attracted significant attention due to their applications as optical[9−19] and electronic[20−23] resonators. Nanoring formation, however, is presently limited by a lack of convenient, inexpensive, and rapid templating methods.[4] This problem has motivated considerable efforts to develop improved patterning techniques.[21,24−44]

One of the most attractive routes for patterning planar surfaces has involved the use of microsphere templates.[4,10,34,38,42,45−49] This technique, which is often called colloidal lithography, has been employed for patterning metals, soft matter, and even organic monolayers in regular arrays on solid substrates. Another recent development has involved the use of capillary lithography to direct metal and semiconductor nanoparticles to specific locations in groves and wells.[3,50] We therefore reasoned that arrays of nanoring structures could be formed with a high degree of control by combining colloidal lithography with capillary lithography. Specifically, ~4 nm CdSe QDs were assembled on planar supported substrates containing hexagonal arrays of polystyrene microspheres ranging in size from 200 nm to 2 μm. Well-ordered nanoparticle rings were left behind on the substrate surface after the microspheres were removed. A schematic diagram of this process is shown in Figure 1. The height and width of the rings could be precisely controlled down to the level of single nanoparticle necklaces. Additionally, the diameter of the rings could be defined by the size of the microspheres used for templating.

RESULTS

Forming Quantum Dot Rings by Evaporative Templating. Hexagonal arrays of nanorings made from CdSe QDs were formed by the procedure outlined in Figure 1. In a first step, an aqueous solution containing 2 μm diameter polystyrene spheres was added to a second aqueous solution containing the CdSe quantum dots. The mixture, which contained ~1×10^{10} spheres/mL and ~1×10^{14} QDs/mL, was then introduced onto various planar supports in a dropwise fashion (~2 μL droplets). The evaporative templating process was allowed to proceed over an approximately 0.2 cm^2 area by drying in air at 23 °C with a relative humidity of ~45%. The microspheres were gently removed from the support by applying and removing a piece of adhesive tape to the

*Address correspondence to cremer@mail.chem.tamu.edu, batteas@mail.chem.tamu.edu, dhson@mail.chem.tamu.edu.

Received for review September 9, 2008 and accepted November 26, 2008.

Published online December 18, 2008. 10.1021/nn800568t CCC: $40.75

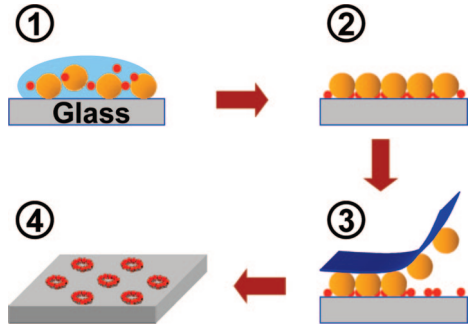

Figure 1. Schematic diagram of the evaporation templating procedure employed for forming CdSe nanorings (red particles) on planar substrates using microsphere templates (orange particles). Note that the drawing is not to scale.

surface. After this, the nanoring array patterns could be directly imaged in air by AFM.

The quality of the patterns depended intimately on the nature of the underlying substrate. For example, hexagonal arrays of nanorings could be formed on glass surfaces; however, some nanoparticles were deposited randomly over the entire surface (Figure 2A). Employing APTMS modified glass left even more material in the background (Figure 2B). This was not surprising as the QDs were acid-terminated and should adhere strongly to the amine-terminated surface *via* electrostatic and hydrogen bonding interactions. Far better results were achieved by using Shipley 1805 coated (Figure 2C) and PVP-modified glass (Figure 2D) substrates. A key difference between these last two coatings was the fact that hexagonal nanoring patterns could be easily washed away from Shipley 1805 coated surfaces, but not from PVP-modified substrates. Such a result suggested that the interactions between the QDs and the Shipley-coated substrates were very weak. On the other hand, PVP-modified substrates appeared to have an intermediate level of interaction with the QDs. Specifically, the interactions were weak enough to prevent most background particle deposition, yet strong enough to resist rinsing away in water. PVP-modified substrates were therefore used in all subsequent studies.

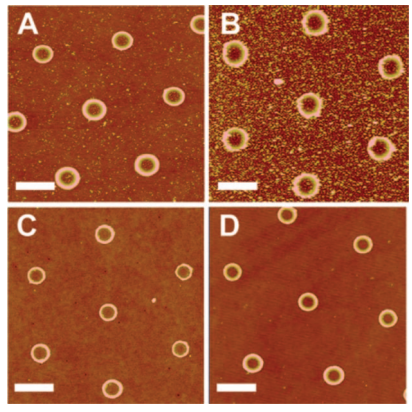

Figure 2. AFM topographical images of CdSe rings on (A) clean glass, (B) APTMS-modified glass, (C) Shipley 1805 photoresist coated glass, and (D) PVP-modified glass. The scale bars are each 1 μm long.

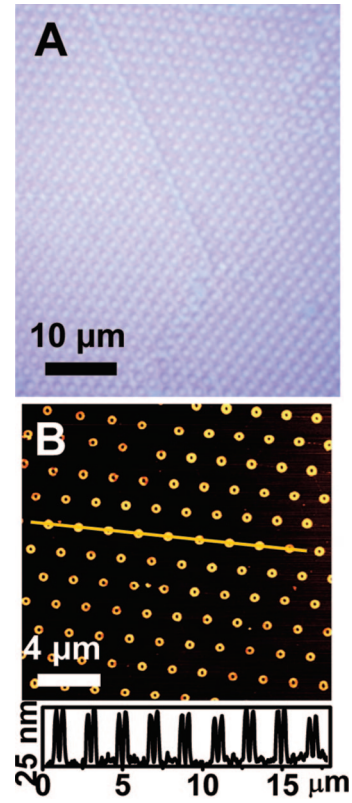

Figure 3. (A) Optical image of polystyrene microspheres on a PVP-modified glass substrate. (B) AFM topographical image and cross section of CdSe nanorings on a PVP-modified glass substrate.

As noted above, the patterns were typically formed over 0.2 cm^2 areas. Before their removal, individual polystyrene microspheres forming hexagonal arrays could be seen optically on PVP-coated surfaces. A 60 μm × 45 μm image of one such array is shown in Figure 3A. A few line and point defects can be clearly seen in the image which is typical for colloidal lithography. Additionally, an AFM image of a 20 μm × 20 μm array of CdSe nanorings is shown in Figure 3B. This approximately represents the upper size limit for a region without major defects. Larger regions inevitably contain the common defects of colloidal lithography.

Verification of Ring Composition. Next, experiments were performed to verify that the nanorings were made from quantum dots. This was done by repeating the evaporative templating experiments without any quantum dots in the aqueous solution. In this case, no material was deposited on the substrate (data not shown). More direct evidence for QD rings comes from confocal fluorescence microscopy/AFM experiments, which can probe the local optical properties of the surface-adsorbed materials with lateral resolution below one micron (488 nm laser excitation and 100 × (0.9 NA) objective). To examine the optical properties of the rings, the sample was immersed in purified water overnight and then rinsed with additional water for 30 s to remove any impurities left on the surface. After this, the sample was dried by blowing N_2 over the surface. Con-

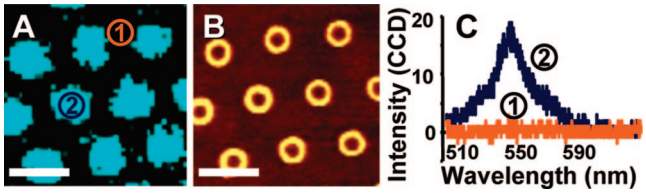

Figure 4. (A) Confocal fluorescence image of CdSe nanorings formed on a PVP-modified glass substrate. (B) An AFM topographical image of the identical area as in (A). The scale bars for both are 2 μm long. (C) Fluorescent emission spectra over the regions labeled "1" and "2" in (A).

focal fluorescence and AFM images of the identical area are shown in panels A and B in Figure 4, respectively. Both images show the hexagonal pattern. The fluorescence signal collected from a single QD ring as well as from a background region is shown in Figure 4C. The QD ring shows peak emission at ~540 nm, which is generally consistent with the fluorescence spectrum for 4 nm CdSe QDs.[51] It should be noted, however, that the peak is ~30 nm blue-shifted compared to the 570 nm peak emission typically found in bulk solution.[52] This may be due to the surface adsorption of the nanoparticles, their partial oxidation in air, or a combination of both phenonmena.[53] To test this hypothesis, CdSe/ZnS nanoparticles with ~7.3 nm diameters were used instead of the smaller CdSe particles (see Supporting Information). In that case, the emission was not blue-shifted with respect to solution conditions due to the improved stability of CdSe/ZnS system (peak maximum at 640 nm). Moreover, AFM line profiles from nanorings of these particles were consistent with their larger size.

Controlling the Geometry of the Ring Arrays. To form rings of varying thickness, the concentration of polystyrene microspheres in solution was held constant at 1×10^{10} spheres/mL, while the concentration of QDs was varied from 1×10^{14} to 1×10^{13} QDs/mL (Figure 5). As can be seen, high concentrations of CdSe quantum dots led to the formation of thicker and higher ring structures, while lower concentrations were associated with thinner rings and lower heights. Specifically, AFM topographic height profiles reveal that a ratio of quantum dots to polymer spheres of 10000:1 led to structures that were at least 6 nanoparticle layers high (Figure 5A). When this ratio was reduced to 4000:1, three-layer high structures were observed (Figure 5B). Ratios of 2000:1 and 1000:1 led to two-layer (Figure 5C) and single-layer structures (Figure 5D), respectively. For the two-layer QD rings shown in Figure 5C, each layer exhibited a thickness of ~5 nm and the stacking structure of the QDs within the rings is readily visible in the image. Moreover, individual QDs could be observed when single monolayer high nanorings were formed (Figure 5D). The width of the structure in Figure 5D was about 20−30 nm. This is consistent with the idea that the apparent width should be dominated by the radius of curvature of the AFM tip, which is substantially greater than the diameter of the CdSe QDs. Line profiles of all single rings revealed that they share roughly the same inner contour structure (Figure 5E), which is consistent with the QDs conforming around individual polymer microspheres during the last stage of the drying process.

In a final set of experiments, we wished to verify that the inner radius of the rings could be varied by tuning the size of the polystyrene spheres. This was accomplished by using spheres with diameters ranging from 2 μm down to 200 nm (Figure 6). A line profile across each ring is shown immediately below the corresponding micrograph. These profiles can be used to measure the contact radius, R_{ring}, as a function of microsphere size. It should be noted that R_{ring} was measured at a height of ~4 nm above the plane of the PVP-coated surface, which should correspond roughly to the middle of the lowest layer of nanoparticles. As can be seen, the inner radius contracted from 133 to 43 nm as the size of the microsphere template was shrunk.

A 10 μm × 10 μm image is shown for each template size (2.5 μm × 2.5 μm for 200 nm microsphere template, Figure 7). As can be seen, ring heights and widths were quite uniform from ring to ring. Moreover, the hexagonal pattern was well preserved in all cases except when the smallest polystyrene microspheres were employed. In this case, the CdSe nanorings were more randomly distributed on the substrate. This occurred because the 200 nm microspheres did not form a uniform hexagonal layer. In other words, the colloidal lithography process did not work perfectly for this smallest sphere size.

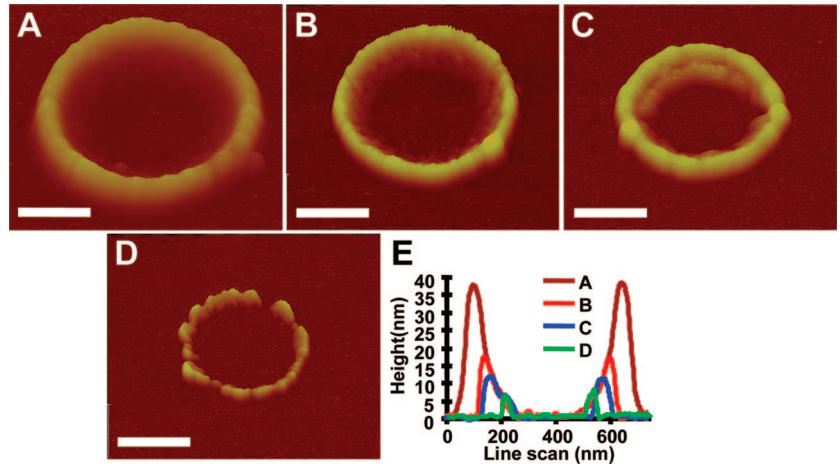

Figure 5. AFM topographical 3D images of CdSe nanorings obtained from solutions using CdSe to polystyrene microsphere ratios of (A) 10000:1, (B) 4000:1, (C) 2000:1, (D) 1000:1. (E) Line profiles through the center of each ring. The scale bars in each image are 200 nm long.

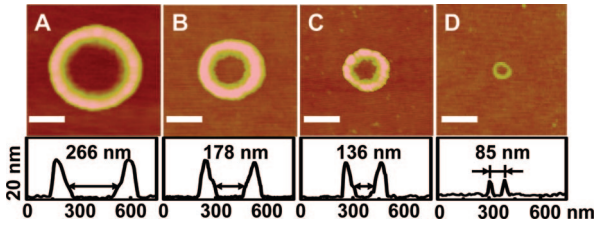

Figure 6. AFM topographical images and the corresponding line profiles from single CdSe nanorings formed with polystyrene spheres having diameters of (A) 2 μm, (B) 1 μm, (C) 600 nm, and (D) 200 nm. All scale bars are 200 nm long. The evaporative templating process was carried out at a CdSe concentration of 2×10^{13} QDs/mL under all conditions. The microsphere concentrations in the initial aqueous solutions were (A) 1×10^{10} spheres/mL, (B) 2×10^{10} spheres/mL, (C) 8×10^{10} spheres/mL, and (D) 3×10^{11} spheres/mL, respectively.

The value of R_{ring} for each microsphere template size could be predicted using a simple hard sphere contact model:

$$R_{ring} = \sqrt{(R_{MS} + R_{QD})^2 - (R_{MS} - R_{QD})^2} \quad (1)$$

where R_{MS} is the radius of the microspheres, and R_{QD} is the radius of quantum dots (Figure 8). Fitting this formula to the four data points from Figure 6 yields a QD radius of ~4.2 nm (Figure 9). Such a value is in excellent agreement with the size of the nanoparticles, whereby the bare CdSe QDs should be ~2 nm in radius and the length of the 16-MHA-capping layer will add slightly more than 2 nm to this value.

DISCUSSION

The advantage of using polystyrene microspheres as nanoscale templates is that the wedge-shaped region between the spheres and the planar substrate provides a convenient location for the deposition of the nonvolatile semiconductor particles. Although spheres have been employed in the present case, it is reasonable to hypothesize that other geometries should work as well. For example, arrays of double lines could be formed by using micron-sized rods as templates. Of course, in that case, the ability to form long-range periodic arrays would depend upon developing methods to properly align the rods over long distances. This technique could also be expanded to pattern numerous other materials besides CdSe QDs. As noted above, however, the surface chemistry must be appropriate for high fidelity nanoring formation (Figure 2). If solute particles adhere too strongly or weakly to the substrate, then patterns will either not form at all or be easily damaged merely by rinsing the surface with water. Below, we briefly outline the forces which need to be taken into consideration.

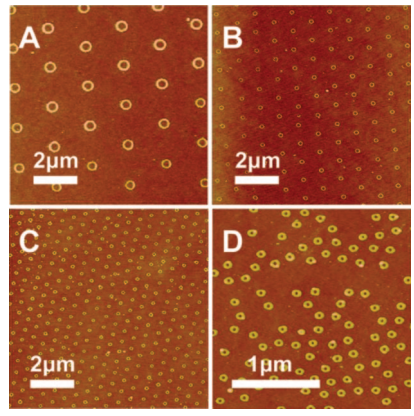

Figure 7. Large area AFM topographical images of CdSe nanorings formed with polystyrene spheres having diameters of (A) 2 μm, (B) 1 μm, (C) 600 nm, and (D) 200 nm. The concentrations of CdSe quantum dots and polystyrene microspheres were the same as in Figure 6.

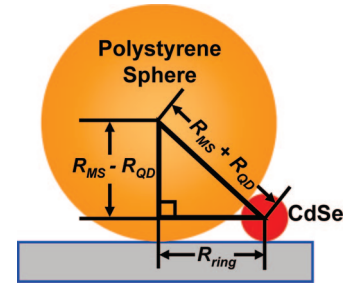

Figure 8. Schematic diagram of the hard sphere contact model employed for calculating the contact radius of the CdSe nanorings. Note that the drawing is not to scale.

The CdSe QDs become sequestered into the wedge region between the polystyrene spheres and the planar substrate during the evaporation process by a delicate interplay of multiple forces. These include capillary forces, $\vec{F}_{cap}$, and nanoparticle/planar substrate adhesion forces, $\vec{F}_{ad}$. Moreover, the surface of the polystyrene spheres possesses a net negative charge in aqueous solution that is counterbalanced by an ionic double layer.[54] Therefore, there should be repulsive interactions between the negatively charged CdSe QDs and the microspheres. This will be manifest as an electrostatic double-layer force, $\vec{F}_{dl}$, whereby the quantum dots can to a first approximation be treated like ions near a charged substrate.[55] Capillary forces act to drag the QDs from the water/air interface toward the wedge region, while the nanoparticle/planar substrate adhesion and double-layer forces act to oppose this move-

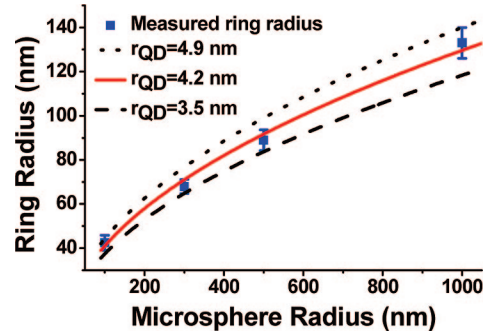

Figure 9. Plot of the CdSe ring radius *versus* the radius of the polystyrene sphere templates. The error bars on the data points are standard deviations from measurements of 20 separate nanorings. Curves were calculated using eq 1.

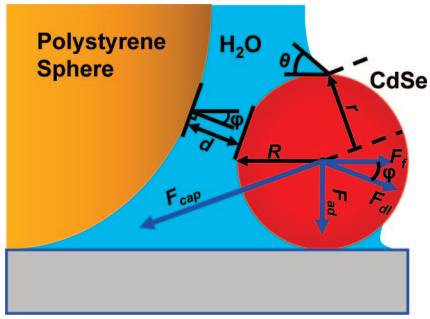

Figure 10. Schematic diagram showing the forces involved in dragging the CdSe quantum dots (shown in red) to the polystyrene spheres (shown in orange). Note that the drawing is not to scale. Moreover, there is almost certainly a hydration layer that coats the entire hydrophilic CdSe quantum dot, which has not been explicitly drawn.

ment. Therefore, the capillary force must exceed the combination of the other two in order for nanorings to form. These forces along with the corresponding frictional drag force, $\vec{F}_f$, which also impedes the movement of the nanoparticles, are summarized in Figure 10 and will be discussed below.

The capillary force, $\vec{F}_{cap}$, can be written as:[3,50,56]

$$\vec{F}_{cap} = 2\pi r\gamma\cos(\theta) \qquad (2)$$

where r is the contact radius of the water/air interface around the quantum dots (Figure 10), γ is the surface tension of water (0.073 N/m at 293 K), and θ is the contact angle, which can be taken to be ~30°.[57] Under these conditions, the maximum radius is limited to the radius of the 16-MHA-capped quantum dots. Therefore, $r_{max} = 4$ nm and $\vec{F}_{cap} \leq 1.6$ nN. Most of this force should be parallel to the plane of the surface; however, a small component will be normal to it. It should also be noted that the total capillary interaction energy between the nanoparticles and microspheres can be estimated by integrating from $r = 0$ to r_{max}.[50] This interaction energy is ~400kT, which suggests that capillary interactions dominate over thermal fluctuations.

The electrostatic double layer force, $\vec{F}_{dl}$, in simplified form can be written as:[58]

$$\vec{F}_{dl} = 2\pi R^2 P e^{-\kappa d} \qquad (3)$$

where R is the nanoparticle radius, P is the surface pressure, κ^{-1} is the Debye length, and d is the separation distance between the surface of a polystyrene sphere and the surface of a quantum dot (Figure 10). This force is somewhat difficult to estimate because the surface charge on the polymer particles can be difficult to measure and vary somewhat from particle to particle. Moreover, the concentration of quantum dots as well as the ionic strength of the solution is constantly increasing during the drying process. Nevertheless, P has been estimated to have an upper bound of 10^7 N/m^2, which corresponds to a surface potential of about 85 mV.[58] Because the QDs are placed in pure water with only hydronium as the counterion, κ^{-1} should be quite large. For pure water, the value would approach 1 μm, which would correspond to the minimum possible screening between a polymer sphere and an individual QD. Therefore, $\vec{F}_{dl} \leq$ ~1 nN.

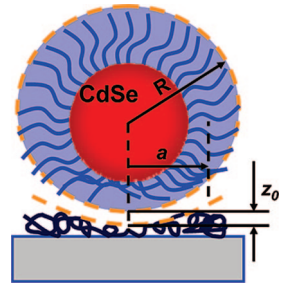

Figure 11. Schematic diagram of a 16-MHA capped CdSe quantum dot in contact with a PVP-modified glass substrate. Note that the drawing is not to scale.

The adhesion force, $\vec{F}_{ad}$, of the nanoparticles to the planar surface, can be approximated as:[59−63]

$$\vec{F}_{ad} = \frac{A}{6z_0^2}\left(R + \frac{a^2}{z_0}\right) \qquad (4)$$

where A is the Hamaker constant for the PVP-QD system in water, R is the CdSe QD radius, z_0 is distance between the edge of the QD and the planar surface, and a is the contact radius. The value of this last constant would presumably be related to the deformation of the 16-MHA-capping layer as well as any deformation in the PVP layer (Figure 11). For 4 nm radius nanoparticles on planar substrates under ambient conditions, the contact radius, a, should be ~2 nm according to continuum elastic theory using the MD (Maugis−Dugdale) transition model.[64] The value of A can be estimated to be approximately 2×10^{-20} J based upon literature values for similar systems.[55,65] Moreover, based upon the Bohr radius of the atoms on the substrate surface and QDs, it is often estimated that z_0 should be ~0.4 nm.[61] This leads to $\vec{F}_{ad} =$ ~0.3 nN for QDs with $R = 4$ nm.

The vectoral addition of $\vec{F}_{dl} + \vec{F}_{ad}$ would have a maximum value of 1.3 nN if they were in the same direction; however, they are not (Figure 10). They would add to approximately 1.1 nN for $\varphi = 80°$. This situation occurs as the first layer of nanoparticles approaches the contact ring. Projecting this magnitude onto the direction perpendicular to the surface normal would provide a force of 0.6 nN opposite to the direction of $\vec{F}_{cap}$. This would make the combination of these two forces considerably smaller than the component of $\vec{F}_{cap}$ which is parallel to the surface. It should be noted that this total vector sum will also be opposed by a kinetic friction component, $\vec{F}_f$, which will also impede the progress of the nanoparticles in the direction of the contact ring.

It is almost certainly the case that $\vec{F}_{cap}$ exceeds $\vec{F}_{dl} + \vec{F}_{ad} + \vec{F}_f$ for all the systems that were examined in Fig-

ure 2. Indeed, rings were formed in all four cases. In Figure 2A,B, however, a significant fraction of CdSe QDs were adsorbed sporadically on the planar substrates rather than at the contact ring. This is almost certainly due to the fact that the adhesion force varies greatly as a function of position. Indeed, defects and related strong interaction sites probably pin the CdSe QDs at specific locations.

Finally, the above calculations lead to the notion that there should be an upper limit to the size of nanoparticles which can be templated by this combined colloidal lithography/capillary lithography technique. This is because the double-layer force will increase faster than the capillary force as the nanoparticle size increases. Specifically, the capillary force increases linearly with nanoparticle radius, while the double-layer force increases as the square of the radius. Based upon the equations above, one would expect the limit to be reached for ~30 nm nanoparticles when 2 μm polymer spheres are employed in conjunction with PVP-coated substrates.

METHODS

Synthesis of CdSe Nanoparticles. Trioctylphospine oxide (TOPO)-capped spherical CdSe nanocrystals were prepared from CdO and Se by employing a well-established solvothermal method.[66] Initially, 250 mg of CdO was heated to 300 °C in a mixture of trioctylphophine oxide (1.15 g), hexadecylamine (2.85 g), and tetradecylphosphonic acid (1.09 g) under a nitrogen atmosphere. After the solution became optically clear, 0.5 g of tributylphosphine was added and the temperature was reduced to 260 °C. Eighty milligrams of selenium dissolved in 0.72 g of tributylphosphine was quickly injected into this mixture to initiate the formation of the nanocrystals. When the desired size of the nanocrystals was reached, the reaction mixture was cooled down to 60 °C and 10 g of nonanoic acid was added. The nanocrystals were purified by repeated precipitation/suspension cycles in methanol and toluene. Passivation of the CdSe nanocrystals with 16-mercaptohexadecanoic acid (16-MHA) was performed by heating the TOPO-capped CdSe nanocrystals in methanolic solutions of 16-MHA and tetraethylammonium hydroxide at 65 °C for 6 h under refluxing conditions.[66] The resulting MHA-capped CdSe nanocrystals were soluble in water and, as expected, exhibited reduced fluorescence compared to TOPO-capped nanocrystals. The average diameter of the CdSe QDs was determined by transmission electron microscopy (TEM) (Figure S1 in Supporting Information). The value was 4.0 ± 0.3 nm, which corresponds only to the semiconductor nanocrystal core and not the 16-MHA coating. This is not surprising, as it is difficult to observe the organic monolayer film by TEM. The concentration of nanoparticle solution was obtained from UV−vis absorption spectrum and the absorption cross section of CdSe nanocrystals.[67]

Microsphere Preparation. Polystyrene microspheres were purchased from Duke Scientific (Fremont, CA). The spheres were repeatedly centrifuged for 5 min at 9300*g* (10000 rpm, Eppendorf Centrifuge 5415D, Hamburg Germany) and resuspended in ultrapure water (18.2 MΩ cm, NANOpure, Barnstead, Dubuque, IA) to remove surfactant molecules from the solution. This centrifugation/resuspension process was typically repeated eight times.

Preparation of Substrates. Glass cover slides (VWR) were cleaned in piranha solution (1:3 H_2O_2/H_2SO_4) and then annealed to 450 °C and held at that temperature for 5 h (*Caution: Piranha is a vigorous oxidant and should be used with extreme caution*). Next, the clean glass slides were modified with three different surface chemistries. These included 3-aminopropyltrimethoxysilane (APTMS, Sigma-Aldrich), Shipley 1805 photoresist (Microchem, Newton MA), and polyvinylpyrrolidone (PVP, Sigma-Aldrich, M_w = 55000). APTMS-modified glass was obtained by placing a recently cleaned glass slide into a 1 mM APTMS/ethanol solution overnight followed by rinsing with ethanol and water. Finally, the slides were dried by blowing compressed nitrogen gas over the surface. Shipley 1805 films were obtained by spin coating a clean glass slide with a 1:5 mixture of Shipley 1805 and Thinner P (Microchem, MA). The substrates were then baked for 1 min at 90 °C followed by further annealing to 120 °C for 1 min. PVP-modified surfaces were prepared by soaking freshly prepared glass substrates in a 1% PVP ethanol solution overnight. The samples were then rinsed sequentially with ethanol and purified water for 1 min each. Finally, the samples were dried by blowing nitrogen gas over the surface.

Surface Imaging. Atomic force microscopy (AFM) images were taken with a Nanoscope IIIa Multimode scanning probe microscope (Veeco-Digital Instruments) using NSC15/noAl ultrasharp tapping mode tips (Micromash; tip radius ~10 nm; average spring constant 40 N/m). Additional images were captured with a WITec Alpha300 combined confocal fluorescence/AFM system to allow for sequential confocal fluorescence and AFM imaging of the same area. For fluorescence imaging, the 488 nm line from an Ar^+ laser was used as the excitation source. Optical micrographs were captured with a Nikon high numerical aperture objective (100×, 0.9 NA). Spectral data were acquired with an Acton triple grating spectrometer imaged onto an Andor Peltier cooled (−70 °C) CCD detector. Fluorescence images were generated from integrated spectra acquired between 500 and 600 nm.

Acknowledgment. We would like to thank Ammon Pickett and Qingsheng Liu for help with TEM imaging as well as discussions. We gratefully acknowledge support from the NIH (R01 GM070622, P.S.C.), the ARO (W911NF-05-1-0494, P.S.C.), the ONR (N00014-08-1-0467, P.S.C.), the Welch Foundation (A-1421, P.S.C.), and the Texas Higher Education Coordinating Board—Advanced Research Program (010366-0006-2006, J.D.B.).

Supporting Information Available: Synthesis methods for CdSe/ZnS, TEM images of CdSe and CdSe/ZnS, fluorescence and AFM images with line profiles, statistical results for particle sizes. This material is available free of charge *via* the Internet at http://pubs.acs.org.

REFERENCES AND NOTES

1. Shipway, A. N.; Katz, E.; Willner, I. Nanoparticle Arrays on Surfaces for Electronic, Optical, and Sensor Applications. *ChemPhysChem* **2000**, *1*, 18–52.
2. Tang, Z.; Kotov, N. A.; Giersig, M. Spontaneous Organization of Single CdTe Nanoparticles into Luminescent Nanowires. *Science* **2002**, *297*, 237–240.
3. Lu, N.; Chen, X.; Molenda, D.; Naber, A.; Fuchs, H.; Talapin, D. V.; Weller, H.; Müller, J.; Lupton, J. M.; Feldmann, J.; *et al.* Lateral Patterning of Luminescent CdSe Nanocrystals by Selective Dewetting from Self-Assembled Organic Templates. *Nano Lett.* **2004**, *4*, 885–888.
4. Henzie, J.; Barton, J. E.; Stender, C. L.; Odom, T. W. Large-Area Nanoscale Patterning: Chemistry Meets Fabrication. *Acc. Chem. Res.* **2006**, *39*, 249–257.
5. Anker, J. N.; Hall, W. P.; Lyandres, O.; Shah, N. C.; Zhao, J.; Van Duyne, R. P. Biosensing with Plasmonic Nanosensors. *Nat. Mater.* **2008**, *7*, 442–453.
6. Murray, C. B.; Kagan, C. R.; Bawendi, M. G. Self-Organization of CdSe Nanocrystallites into Three-Dimensional Quantum Dot Superlattices. *Science* **1995**, *270*, 1335–1338.
7. Daniel, M.-C.; Astruc, D. Gold Nanoparticles: Assembly, Supramolecular Chemistry, Quantum-Size-Related Properties, and Applications toward Biology, Catalysis, and Nanotechnology. *Chem. Rev.* **2004**, *104*, 293–346.

8. Coe-Sullivan, S.; Steckel, J. S.; Woo, W.-K.; Bawendi, M. G.; Bulović, V. Large-Area Ordered Quantum-Dot Monolayers *via* Phase Separation During Spin-Casting. *Adv. Funct. Mater.* **2005**, *15*, 1117–1124.
9. Absil, P. P.; Hryniewicz, J. V.; Little, B. E.; Cho, P. S.; Wilson, R. A.; Joneckis, L. G.; Ho, P.-T. Wavelength Conversion in GaAs Micro-Ring Resonators. *Opt. Lett.* **2000**, *25*, 554–556.
10. Aizpurua, J.; Hanarp, P.; Sutherland, D. S.; Käll, M.; Bryant, G. W.; García de Abajo, F. J. Optical Properties of Gold Nanorings. *Phys. Rev. Lett.* **2003**, *90*, 057401-1–057401-4.
11. Aizpurua, J.; Blanco, L.; Hanarp, P.; Sutherland, D. S.; Käll, M.; Bryant, G. W.; García de Abajo, F. J. Light Scattering in Gold Nanorings. *J. Quant. Spectrosc. Radiat. Transf.* **2004**, *89*, 11–16.
12. Heebner, J. E.; Lepeshkin, N. N.; Schweinsberg, A.; Wicks, G. W.; Boyd, R. W.; Grover, R.; Ho, P.-T. Enhanced Linear and Nonlinear Optical Phase Response of AlGaAs Microring Resonators. *Opt. Lett.* **2004**, *29*, 769–771.
13. Kim, S.; Jung, J.-M.; Choi, D.-G.; Jung, H.-T.; Yang, S.-M. Patterned Arrays of Au Rings for Localized Surface Plasmon Resonance. *Langmuir* **2006**, *22*, 7109–7112.
14. Bozhevolnyi, S. I.; Volkov, V. S.; Devaux, E.; Laluet, J.-Y.; Ebbesen, T. W. Channel Plasmon Subwavelength Waveguide Components Including Interferometers and Ring Resonators. *Nature* **2006**, *440*, 508–511.
15. Pauzauskie, P. J.; Sirbuly, D. J.; Yang, P. Semiconductor Nanowire Ring Resonator Laser. *Phys. Rev. Lett.* **2006**, *96*, 143903-1–143903-4.
16. Sheridan, A. K.; Clark, A. W.; Glidle, A.; Cooper, J. M.; Cumming, D. R. S. Multiple Plasmon Resonances From Gold Nanostructures. *Appl. Phys. Lett.* **2007**, *90*, 143105-1–143105-3.
17. Ramakrishna, G.; Dai, Q.; Zou, J.; Huo, Q., III. Interparticle Electromagnetic Coupling in Assembled Gold-Necklace Nanoparticles. *J. Am. Chem. Soc.* **2007**, *129*, 1848–1849.
18. Jung, K.-Y.; Teixeira, F. L.; Reano, R. M. Au/SiO_2 Nanoring Plasmon Waveguides at Optical Communication Band. *J. Lightwave Technol.* **2007**, *25*, 2757–2765.
19. Rochholz, H.; Bocchio, N.; Kreiter, M. Tuning Resonances on Crescent-Shaped Noble-Metal Nanoparticles. *New J. Phys.* **2007**, *9*, 53-1–53-18.
20. Frens, G. Controlled Nucleation For Regulation Of Particle-Size In Monodisperse Gold Suspensions. *Nat. Phys. Sci.* **1973**, *241*, 20–22.
21. Lorke, A.; Luyken, R. J.; Govorov, A. O.; Kotthaus, J. P.; Garcia, J. M.; Petroff, P. M. Spectroscopy of Nanoscopic Semiconductor Rings. *Phys. Rev. Lett.* **2000**, *84*, 2223–2226.
22. Jariwala, E. M. Q.; Mohanty, P.; Ketchen, M. B.; Webb, R. A. Diamagnetic Persistent Current in Diffusive Normal-Metal Rings. *Phys. Rev. Lett.* **2001**, *86*, 1594–1597.
23. Pederiva, F.; Emperador, A.; Lipparini, E. Electron Localization in Low-Density Quantum Rings. *Phys. Rev. B* **2002**, *66*, 165314-1–165314-6.
24. Ohara, P. C.; Heath, J. R.; Gelbart, W. M. Self-Assembly of Submicrometer Rings of Particles from Solutions of Nanoparticles. *Angew. Chem., Int. Ed. Engl.* **1997**, *36*, 1077–1080.
25. Stowell, C.; Korgel, B. A. Self-Assembled Honeycomb Networks of Gold Nanocrystals. *Nano Lett.* **2001**, *1*, 595–600.
26. Odom, T. W.; Thalladi, V. R.; Love, J. C.; Whitesides, G. M. Generation of 30−50 nm Structures Using Easily Fabricated, Composite PDMS Masks. *J. Am. Chem. Soc.* **2002**, *124*, 12112–12113.
27. Kalinin, S. V.; Bonnell, D. A.; Alvarez, T.; Lei, X.; Hu, Z.; Ferris, J. H.; Zhang, Q.; Dunn, S. Atomic Polarization and Local Reactivity on Ferroelectric Surfaces: A New Route toward Complex Nanostructures. *Nano Lett.* **2002**, *2*, 589–593.
28. Garno, J. C.; Yang, Y.; Amro, N. A.; Cruchon-Dupeyrat, S.; Chen, S.; Liu, G.-Y. Precise Positioning of Nanoparticles on Surfaces Using Scanning Probe Lithography. *Nano Lett.* **2003**, *3*, 389–395.
29. Heydermana, L. J.; David, C.; Kläui, M.; Vaz, C. A. F.; Bland, J. A. C. Nanoscale Ferromagnetic Rings Fabricated by Electron-Beam Lithography. *J. Appl. Phys.* **2003**, *93*, 10011–10013.
30. Babayan, Y.; Barton, J. E.; Greyson, E. C.; Odom, T. W. Templated and Hierarchical Assembly of CdSe/ZnS Quantum Dots. *Adv. Mater.* **2004**, *16*, 1341–1345.
31. McLellan, J. M.; Geissler, M.; Xia, Y. Edge Spreading Lithography and Its Application to the Fabrication of Mesoscopic Gold and Silver Rings. *J. Am. Chem. Soc.* **2004**, *126*, 10830–10831.
32. Yan, F.; Goedel, W. A. Preparation of Mesoscopic Gold Rings Using Particle Imprinted Templates. *Nano Lett.* **2004**, *4*, 1193–1196.
33. Saunders, A. E.; Shah, P. S., Jr.; Hanrath, T.; Hwang, H. S.; Lim, K. T.; Johnston, K. P.; Korgel, B. A. Inverse Opal Nanocrystal Superlattice Films. *Nano Lett.* **2004**, *4*, 1943–1948.
34. Geissler, M.; McLellan, J. M.; Chen, J.; Xia, Y. Side-by-Side Patterning of Multiple Alkanethiolate Monolayers on Gold by Edge-Spreading Lithography. *Angew. Chem., Int. Ed.* **2005**, *44*, 3596–3600.
35. Chen, P.; Chua, S. J.; Wang, Y. D.; Sander, M. D.; Fonstad, C. G. InGaN Nanorings and Nanodots by Selective Area Epitaxy. *Appl. Phys. Lett.* **2005**, *87*, 143111-1–143111-3.
36. Gates, B. D.; Xu, Q.; Stewart, M.; Ryan, D.; Willson, C. G.; Whitesides, G. M. New Approaches to Nanofabrication: Molding, Printing, and Other Techniques. *Chem. Rev.* **2005**, *105*, 1171–1196.
37. Lin, Z.; Granick, S. Patterns Formed by Droplet Evaporation from a Restricted Geometry. *J. Am. Chem. Soc.* **2005**, *127*, 2816–2817.
38. Yang, S.-M.; Jang, S. G.; Choi, D.-G.; Kim, S.; Yu, H. K. Nanomachining by Colloidal Lithography. *Small* **2006**, *2*, 458–475.
39. Hampton, J. R.; Dameron, A. A.; Weiss, P. S. Double-Ink Dip-Pen Nanolithography Studies Elucidate Molecular Transport. *J. Am. Chem. Soc.* **2006**, *128*, 1648–1653.
40. Xu, J.; Xia, J.; Lin, Z. Evaporation-Induced Self-Assembly of Nanoparticles from a Sphere-on-Flat Geometry. *Angew. Chem., Int. Ed.* **2007**, *46*, 1860–1863.
41. Khanal, B. P.; Zubarev, E. R. Rings of Nanorods. *Angew. Chem., Int. Ed.* **2007**, *46*, 2195–2198.
42. Li, J.-R.; Garno, J. C. Elucidating the Role of Surface Hydrolysis in Preparing Organosilane Nanostructures *via* Particle Lithography. *Nano Lett.* **2008**, *8*, 1916–1922.
43. Park, S.; Wang, J.-Y.; Kim, B.; Russell, T. P. From Nanorings to Nanodots by Patterning with Block Copolymers. *Nano Lett.* **2008**, *8*, 1667–1672.
44. Zhang, L.; Si, H.-Y.; Zhang, H.-L. Highly Ordered Fluorescent Rings by "Breath Figures" on Patterned Substrates Using Polymer-Free CdSe Quantum Dots. *J. Mater. Chem.* **2008**, *18*, 2660–2665.
45. Hulteen, J. C.; Van Duyne, R. P. Nanosphere Lithography: A Materials General Fabrication Process for Periodic Particle Array Surfaces. *J. Vac. Sci. Technol., A* **1995**, *13*, 1553–1558.
46. Winzer, M.; Kleiber, M.; Dix, N.; Wiesendanger, R. Fabrication of Nano-Dot- and Nano-Ring-Arrays by Nanosphere Lithography. *Appl. Phys. A: Mater. Sci. Process.* **1996**, *63*, 617–619.
47. Garno, J. C.; Amro, N. A.; Wadu-Mesthrige, K.; Liu, G.-Y. Production of Periodic Arrays of Protein Nanostructures Using Particle Lithography. *Langmuir* **2002**, *18*, 8186–8192.
48. Li, J.-R.; Henry, G. C.; Garno, J. C. Fabrication of Nanopatterned Films of Bovine Serum Albumin and Staphylococcal Protein A Using Latex Particle Lithography. *Analyst* **2006**, *131*, 244–250.
49. Liao, W.-S.; Chen, X.; Chen, J.; Cremer, P. S. Templating Water Stains for Nanolithography. *Nano Lett.* **2007**, *7*, 2452–2458.
50. Cui, Y.; Björk, M. T.; Liddle, J. A.; Sönnichsen, C.; Boussert, B.; Alivisatos, A. P. Integration of Colloidal Nanocrystals into Lithographically Patterned Devices. *Nano Lett.* **2004**, *4*, 1093–1098.

51. Empedocles, S. A.; Norris, D. J.; Bawendi, M. G. Photoluminescence Spectroscopy of Single CdSe Nanocrystallite Quantum Dots. *Phys. Rev. Lett.* **1996**, *77*, 3873–3876.
52. Derfus, A. M.; Chan, W. C. W.; Bhatia, S. N. Probing the Cytotoxicity of Semiconductor Quantum Dots. *Nano Lett.* **2004**, *4*, 11–18.
53. Katari, J. E. B.; Colvin, V. L.; Alivisatos, A. P. X-ray Photoelectron Spectroscopy of CdSe Nanocrystals with Applications to Studies of the Nanocrystal Surface. *J. Phys. Chem.* **1994**, *98*, 4109–4117.
54. Tarhan, I˙. I˙.; Watson, G. H. Photonic Band Structure of fcc Colloidal Crystals. *Phys. Rev. Lett.* **1996**, *76*, 315–318.
55. Israelachvili, J. *Intermolecular & Surface Forces*, 2nd ed.; Academic Press Inc.: San Diego, CA, 1991.
56. Rabideau, B. D.; Pell, L. E.; Bonnecaze, R. T.; Korgel, B. A. Observation of Long-Range Orientational Order in Monolayers of Polydisperse Colloids. *Langmuir* **2007**, *23*, 1270–1274.
57. Bain, C. D.; Whitesides, G. M. A Study by Contact Angle of the Acid-Base Behavior of Monolayers Containing ω-Mercaptocarboxylic Acids Adsorbed on Gold: An Example of Reactive Spreading. *Langmuir* **1989**, *5*, 1370–1378.
58. Attard, P. Interaction and Deformation of Viscoelastic Particles: Nonadhesive Particles. *Phys. Rev. E* **2001**, *63*, 061604-1–061604-9.
59. Ge, G.; Brus, L. Evidence for Spinodal Phase Separation in Two-Dimensional Nanocrystal Self-Assembly. *J. Phys. Chem. B* **2000**, *104*, 9573–9575.
60. Rabani, E. An Interatomic Pair Potential for Cadmium Selenide. *J. Chem. Phys.* **2002**, *116*, 258–262.
61. Bakhtari, K.; Guldiken, R. O.; Busnaina, A. A.; Park, J.-G. Experimental and Analytical Study of Submicrometer Particle Removal from Deep Trenches. *J. Electrochem. Soc.* **2006**, *153*, C603–C607.
62. Bakhtari, K.; Guldiken, R. O.; Makaram, P.; Busnaina, A. A.; Park, J.-G. Experimental and Numerical Investigation of Nanoparticle Removal Using Acoustic Streaming and the Effect of Time. *J. Electrochem. Soc.* **2006**, *153*, G846–G850.
63. Chein, R.; Liao, W. Modeling of Particle Removal Using Non-Contact Brush Scrubbing in Post-CMP Cleaning Processes. *J. Adhesion* **2006**, *82*, 555–575.
64. Grobelny, J.; Pradeep, N.; Kim, D.-I. Estimation of Contact Area of Nanoparticles in Chains Using Continuum Elastic Contact Mechanics. *J. Nanopart. Res.* **2008**, DOI 10.1007/s11051-008-9434-8.
65. Gu, Y. Experimental Determination of the Hamaker Constants for Solid-Water-Oil Systems. *J. Adhesion Sci. Technol.* **2001**, *15*, 1263–1283.
66. Peng, Z. A.; Peng, X. Formation of High-Quality CdTe, CdSe, and CdS Nanocrystals Using CdO as Precursor. *J. Am. Chem. Soc.* **2001**, *123*, 183–184.
67. Leatherdale, C. A.; Woo, W.-K.; Mikulec, F. V.; Bawendi, M. G. On the Absorption Cross Section of CdSe Nanocrystal Quantum Dots. *J. Phys. Chem. B* **2002**, *106*, 7619–7622.